Electronic Supplementary Material (ESI) for Nanoscale.


# Constructing $CeO_2$/nitrogen-doped carbon quantum dots/g-$C_3N_4$ heterojunction photocatalysts for highly efficient visible light photocatalysis

Houjuan Qi[a], Cai Shi[a], Xiaona Jiang[a], Min Teng[a], Zhe Sun[a],

Zhanhua Huang[a*], Duo Pan[b,c],Shouxin Liu[a], Zhanhu Guo[b*]

a. Key Laboratory of Bio-based Material Science & Technology（Northeast Forestry University），College of material science and engineering, Ministry of Education，Harbin 150040, China

b. Integrated Composites Laboratory (ICL), Department of Chemical and Bimolecular Engineering, University of Tennessee, Knoxville, Tennessee 37996, United States

c. Key Laboratory of Materials Processing and Mold (Zhengzhou University), Ministry of Education, National Engineering Research Center for Advanced Polymer Processing Technology, Zhengzhou University, Zhengzhou, China

***Corresponding authors.**

**E-mail address:** huangzh1975@163.com (Z. Huang);

zguo10@utk.edu (Z. Guo)

## Experimental Sections

### *Materials*

Ammonium oxalate (AO, AR) and ammonia were purchased from Tianjin Kemiou Chemical Reagent Co. Ltd., China. 1,4-benzoquinone (BQ, 98%) was purchased from Sinopharm Chemical ReagentCo., Ltd. Triton X-100 (BR) was produced from Shanghai McLean biochemical technology co., LTD. $Ce(NO_3)_3 \cdot 6H_2O$ (98.5%) was purchased from Tianjin Zhiyuan chemical reagent co. LTD. Melamine (AR), ethanol (95%) and $Na_2SO_4$ (99%) were procured from Tianjin Guangfu Fine Chemical Research Institute. Dimethyl sulfoxide (AR), 2-propanol (99%), tetracycline (TC, 99%), $H_2SO_4$ (98%) and 5,5-dimethyl-1-pyrroline N-oxide (DMPO, 97%) were bought from Tianjin Bodi Chemical Co., Ltd., Tianjin tianli chemical reagent co. LTD., Shandong west Asia chemical industry co. LTD, Xilong science and technology co. LTD and Cool chemical technology co. LTD, respectively. Nitrogen-doped carbon quantum dots (NCQDs, Fungal cellulose) was homemade in the lab by the hydrothermal method.

### *Characterization*

UV−vis absorption spectroscopy: the ultraviolet-visible spectrums were measured using TU-1950 UV-vis spectrophotometer (Beijing Purkinje general instrument Co. Ltd., China). TC showed good Uv-vis response at 354 nm.

UV–vis diffuse reflectance measurements (DSR)：the ultraviolet visible diffuse reflection spectra were measured in range of 200 – 800 nm by TU-1900 spectrophotometer (Beijing Purkinje General Instrument Co., Ltd. China).

Photoluminescence spectroscopy (PL): photoluminescence spectrum of samples was measured on a Cary-Eclipse fluorescence spectrophotometer (AGILENT, Australia). The excitation wavelength of sample is 325 nm at room temperature.

Fourier-transform infrared spectroscopy (FTIR): the FTIR spectroscopy was performed with an iS 10 FTIR spectrometer (Thermo Nicolet Co., Waltham, MA, USA). The wavenumber range of 4000 $cm^{-1}$ to 500 $cm^{-1}$ with the number 32 scans in the resolution of 4 $cm^{-1}$.

X-ray Photoelectron Spectroscopy (XPS): XPS was characterized by K-Alpha (PHI5700, Thermo Electron Corporation, USA). The non-monochromatic Al X-rays at 140 W was used as the primary excitation. The C1s peak at 284.6 eV as an internal standard was corrected the binding energy due to the relative surface charging.

Transmission electron microscope (TEM) and high-resolution TEM (HRTEM): the samples were carried out on JEM-2100 transmission electron microscope (LJEMOC, Japan). The samples were prepared by dropping photocatalyst dispersion in ethanol onto carbon coated copper grids and letting the ethanol evaporate at room temperature. TEM images, HRTEM images, and selected area electron diffraction (SAED) were performed with a JEM-2100 transmission electron microscope (LJEMOC, Japan) operating at an accelerating voltage of 200 kV.

Brunauer–Emmett–Teller (BET): $N_2$ adsorption-desorption isotherms and pore-size distributions were studied by a nitrogen adsorption analyzer (ASAP2020, Micromeritics, USA).

X-ray diffraction (XRD): XRD were recorded by a Rigaku D/Max 2200 X-ray

diffractometer with a scanning rate of 5°/min. the 2θ was formed 5° to 80° at room temperature. The X-ray tube using Cu Kα radiation (λ=1.5418 Å) was operated at 40 mA and 40 kV.

Scanning electron microscope (SEM): the samples images were taken with a microscope (Quanta200, FEI, USA) operated at 12.5 kV. To make the samples conductive, sample surfaces were coated with a thin layer of gold using an ion sputter coater prior to the SEM analysis.

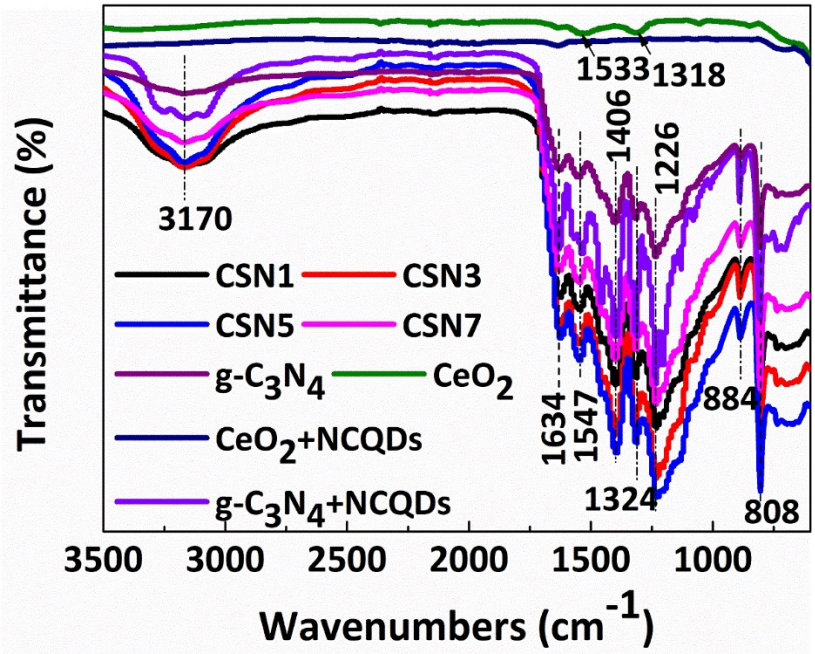


**Fig. S1** FT-IR patterns for g-$C_3N_4$, g-$C_3N_4$+NCQDs, $CeO_2$, $CeO_2$+NCQDs and CSN composites

The interaction between the NCQDs, $CeO_2$ and g-$C_3N_4$ was first investigated by FTIR spectra. As shown in Fig. S1, the band at 808 $cm^{-1}$ could be attributed to the breathing mode of triazine units [1]. The bands region of 1200-1650 $cm^{-1}$ were consisted with stretching vibration of the CN heterocycle. The peaks at 1634 $cm^{-1}$ are attributable to C=N stretching vibration modes, while the 1226, 1324, 1406 and 1547 $cm^{-1}$ can be

ascribed to aromatic C-N stretching vibration modes [2]. The broad band centered at 3170 $cm^{-1}$ can be assigned to the stretching mode of the NH bond. The characteristic absorption peak of Ce-O bending vibration was appeared at 850 $cm^{-1}$ [3]. However, the FTIR spectra of CSN composite shows no obvious characteristic peaks of NCQDs and $CeO_2$, which may be low content of NCQDs and $CeO_2$.

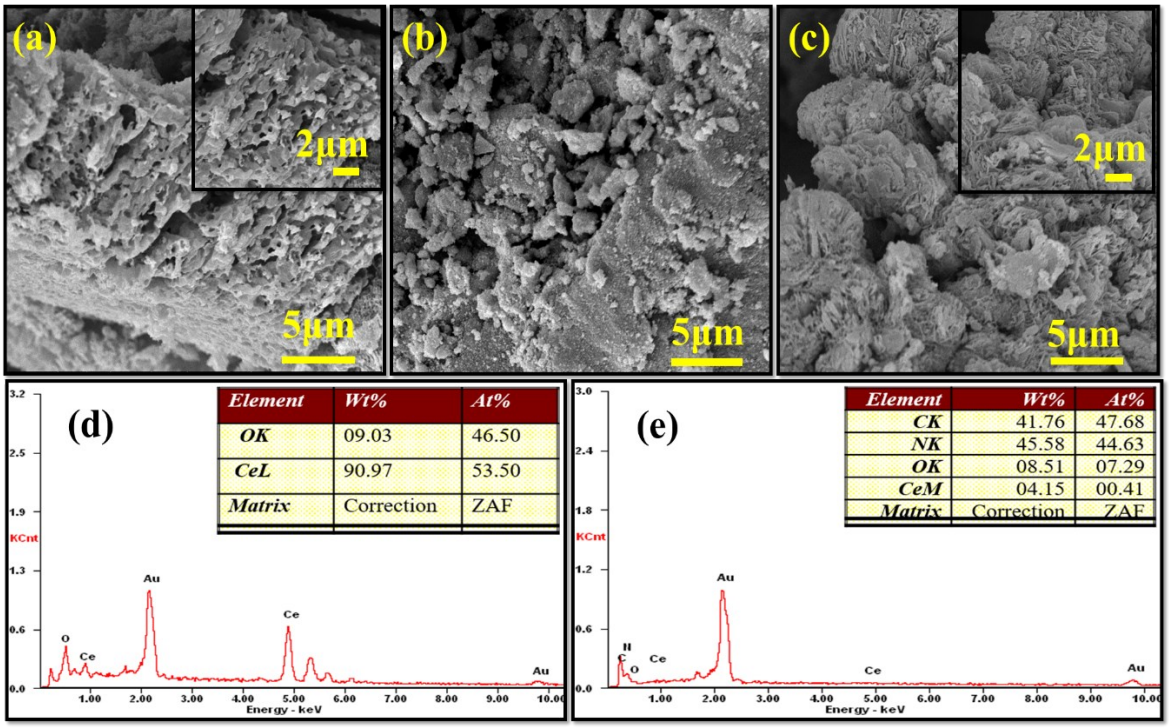


**Fig. S2** SEM images of bulk g-$C_3N_4$ (a, insert is high magnification images of g-$C_3N_4$), $CeO_2$ (b) and CSN5 sample (c, insert is high magnification images of CSN5).

**Calculation of conduction band (CB) and valence band (VB)**

The energy band of samples were estimated by Kubelka-Munk theory [2, 4]. The formula $\alpha hv = A(hv–Eg)^n$, where α, h, v, A, and Eg are the absorption coefficient, Planck's constant, the light frequency, a constant, and the band gap, respectively. The n values of direct and indirect semiconductors are 1/2 and 2, respectively.

$$E_{CB} = \chi - E^e - 0.5\ E_g \quad (1)$$

$$E_{VB} = E_{CB} + E_g \quad (2)$$

where $E_e$ is the energy of free electrons on the hydrogen scale (approx. 4.5 eV); $\chi$ is the electronegativity of the semiconductor, estimated from the geometric mean of the electronegativity of the constituent atoms (the values were 5.56 eV and 4.74 eV for $CeO_2$ and g-$C_3N_4$, respectively), [5-8] and $E_g$ is the band gap energy of the semiconductor.

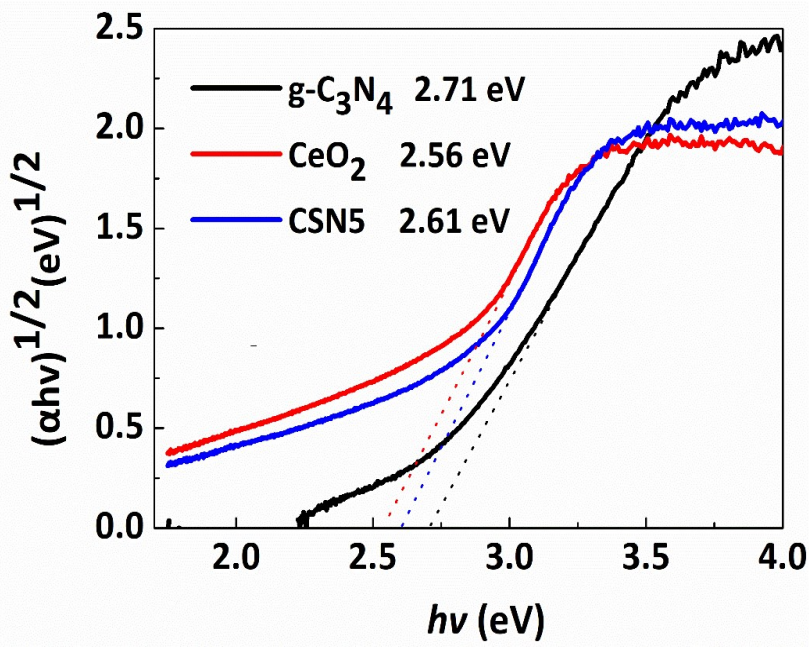


**Fig. S3** The plot of $(\alpha h\nu)^{1/2}$ vs. $h\nu$ for photocatalyst band-gap.

**Table S1** Calculation of the CB and VB Potentials of g-$C_3N_4$ and $CeO_2$

| Samples | $\chi$ | $E_g$ (eV) | $E_{CB}$ (eV) | $E_{VB}$ (eV) |
|---|---|---|---|---|
| $CeO_2$ | 5.56 | 2.56 | – 0.22 | 2.34 |
| g-$C_3N_4$ | 4.74 | 2.71 | –1.115 | 1.595 |

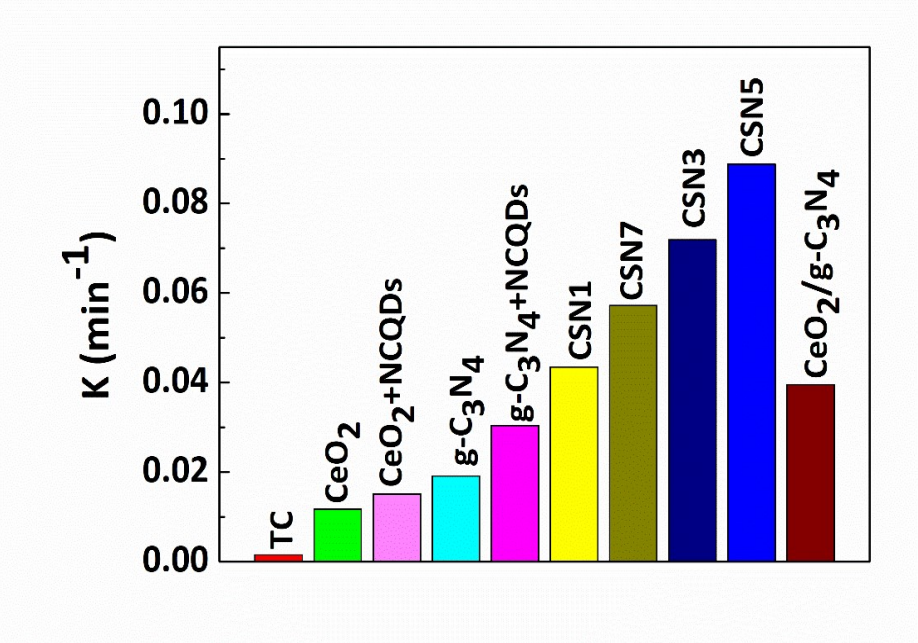


**Fig. S4** Values of reaction rate constants of TC degradation by different photocatalysts.

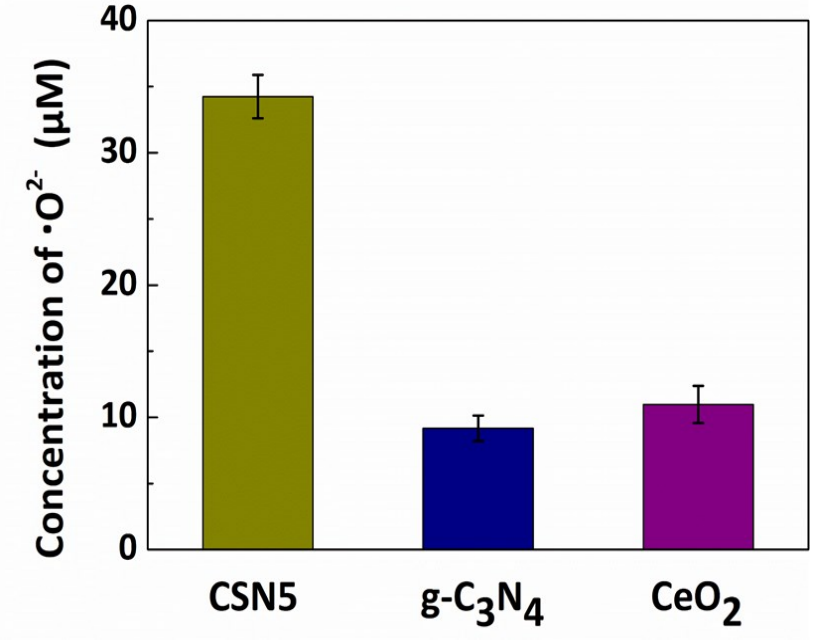


**Fig. S5** The concentration of $\bullet O_2^-$ of CSN5, g-$C_3N_4$, and $CeO_2$.

**Table S2** Barret-Joyner-Halenda (BJH) pore size of different photocatalysts

| Samples | $S_{BET}$ ($m^2/g$) | V ($cm^3/g$) | d(nm) |
|---|---|---|---|
| CSN1 | 49.56 | 0.0642 | 12.33 |
| CSN3 | 42.88 | 0.1948 | 10.55 |
| CSN5 | 38.28 | 0.1422 | 11.47 |
| CSN7 | 20.82 | 0.1175 | 12.28 |
| $CeO_2$ | 45.56 | 0.1556 | 8.24 |
| $CeO_2$+NCQDs | 39.59 | 0.1121 | 11.32 |
| g-$C_3N_4$+NCQDs | 64.56 | 0.0804 | 13.09 |
| g-$C_3N_4$ | 74.61 | 0.2619 | 14.04 |

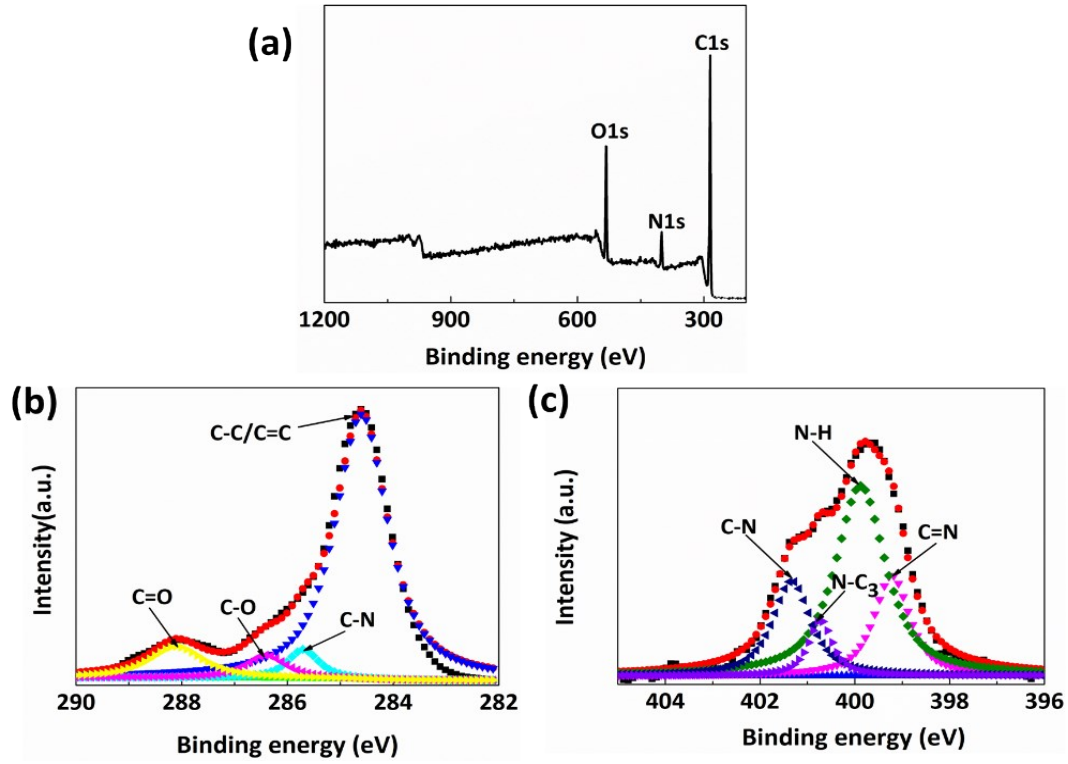


**Fig. S6** XPS survey spectrum of NCQDs (a); High-resolution C1s peaks and fitting curves (b); High-resolution N1s peaks and fitting curves (c).

The C, N and O elements are shown in Fig. S6a. The four peaks at 284.6, 285.7, 286.7and 288.1 eV in the high-resolution C1s spectrum (Fig. S6b) are ascribed to C–C/C=C, C–N, C–O, and C=O groups, respectively.[9-11] In the high-resolution N1s spectrum (Fig. S6c), the peaks at approximately 399.1, 399.7, 400.5, and 401.3 eV correspond to the C=N, N-H, N-$C_3$, and C-N groups, respectively.[12-13]

**Table S3** The photodegradation properties towards various $CeO_2$-based photocatalysts.

| Photocatalysts | Preparation method | Photodegradation | Degradation efficiency | Reference |
|---|---|---|---|---|
| $Ag_2O/CeO_2$ | Thermal decomposition | Enrofloxacin | 87.11% in 120 min | [14] |
| $Ag/AgCl–CeO_2$ | Calcination | Norfloxacin | 91% in 90 min | [15] |
| $CeO_2/g\text{-}C_3N_4$ | Wet-chemical | 2,4-dichlorophenol | 57 % in120 min | [16] |
| $CeO_2$/attapulgite /$g\text{-}C_3N_4$ | Electrostatic-induced self-assembly | Dibenzothiophene | 98% in180 min | [17] |
| $Co_3O_4\text{-}CeO_2$ | Co-precipitation | Diclofenac | 90% in180 min | [18] |
| $CeO_2$QDs/BiOX | Low-temperature synthesis | TC | 97% in120 min | [19] |
| ZnO/$CeO_2$@HNTs | Wet-calcination | TC | 94% in 90 min | [3] |
| $AgI/CeO_2$ | Deposition–precipitation | TC | 94.34% in 60 min | [20] |
| $CeO_2/Bi_2MoO_6$ | In-situ precipitation | TC | 78.7% in 120 min | [21] |
| $CeO_2$/NCQDs/$g\text{-}C_3N_4$ | High-calcination and hydrothermal | TC | 100% in 60 min | This work |

**References**


1. L. Li, D. Deng, S. Huang, H. Song, K. Xu, L. Zhang, Y. Lv, *Anal. Chem.,* 2018, **90**, 9598-9605.

2. L. Shao, D. Jiang, P. Xiao, L. Zhu, S. Meng, M. Chen, *Appl. Catal. B- Environ.,* 2016, **198**, 200-210.

3. Z. Ye, J. Li, M. Zhou, H. Wang, Y. Ma, P. Huo, L. Yu, Y. Yan, *Chem. Eng. J.,* 2016, **304**, 917-933.

4. H. Wang, X. Yuan, H. Wang, X. Chen, Z. Wu, L. Jiang, W. Xiong, G. Zeng, *Appl. Catal. B-Environ.,* 2016, **193**, 36-46.

5. W. Liu, J. Zhou, J. Yao, *Ecotoxicol. Environ. Safe.,* 2020, **190**, 110062.

6. W. Zou, B. Deng, X. Hu, Y. Zhou, Y. Pu, S. Yu,; K. Ma, J. Sun, H. Wan, L. Dong, *Appl. Catal. B-Environ.,* 2018, **238**, 111-118.

7. N. Tian, H. Huang, C. Liu, F. Dong, T. Zhang, X. Du, S. Yu, Y. Zhang, *J. Mater. Chem. A,* 2015, **3**, 17120-17129.

8. Y. Yuan, G. F. Huang, W. Y. Hu, D. N. Xiong, B. X. Zhou, S. Chang, W. Q. Huang, *J. Phys. Chem. Solids,* 2017, **106**, 1-9.

9. H. Qi, M. Teng, M. Liu, S. Liu, J. Li, H. Yu, C. Teng, Z. Huang, H. Liu, Q. Shao, A. Umar, T. Ding, Q. Gao, Z. Guo, *J. Colloid Interface Sci.,* 2019, **539**, 332-341.

10. N. T. N. Anh, A. D. Chowdhury, R. A. Doong, *Sen. Actuat. B-Chem.,* 2017, **252**, 1169-1178.

11. Z. Song, F. Quan, Y. Xu, M. Liu, L. Cui, J. Liu, *Carbon,* 2016, **104**, 169-178.

12. C. Shi, H. Qi, R. Ma, Z. Sun, L. Xiao, G. Wei, Z. Huang, S. Liu, J. Li, M. Dong, J. Fan,; Z. Guo, *Mater. Sci. Engin. C,* 2019, **105**, 110132.

13. M. Xue, L. Zhang, M. Zou, C. Lan,; Z. Zhan, S. Zhao, *Sen. Actuat. B-Chem.,* 2015, **219**, 50-56.

14. X. J. Wen, C. G. Niu, L. Zhang, C. Liang, G. M. Zeng, *Appl. Catal. B- Environ.,* 2018, **221**, 701-714.

15. X. J. Wen, C. G. Niu, D. W. Huang, L. Zhang, C. Liang, G. M. Zeng, *J. Catal.,* 2017, **355**, 73-86.

16. M. Humayun, Z. Hu, A. Khan, W. Cheng, Y. Yuan, Z. Zheng,; Q. Fu, W. Luo, *J. Hazard. Mater.,* 2019, **364**, 635-644.

17. X. Li, W. Zhu, X. Lu, S. Zuo, C. Yao, C. Ni, *Chem. Engin. J.,* 2017, **326**, 87-98.

18. G. Xian, G. Zhang, H. Chang, Y. Zhang, Z. Zou, X. Li, *J. Environ. Manage.,* 2019, **234**, 265-272.

19. J. Yang, Y. Liang, K. Li, G. Yang, S. Yin, *Appl. Catal. B-Environ.,* 2019, **250**, 17-30.

20. X. J. Wen, C. G. Niu, M. Ruan, L. Zhang, G. M. Zeng, *J. Colloid Interface Sci.,* 2017, **497,** 368-377.

21. S. Li, S. Hu, W. Jiang, Y. Liu, Y. Zhou, J. Liu, Z. Wang, *J. Colloid Interface Sci.* 2018, **530**, 171-178.